KLOE NOTE n^o 217
October 2007

Precise measurement of the η mass.

B. Di Micco

Università degli Studi di Roma Tre
I.N.F.N sezione di Roma III

Abstract

An integrated luminosity of 410 pb^{-1}, corresponding to $\sim$ 17 million of η events from the $\Phi \to \eta\gamma$ radiative decay, has been analyzed to measure the η mass using the decay $\eta \to \gamma\gamma$. The signal is searched in events with 3 photons in the final state. To improve the 2γ invariant mass resolution, we perform a kinematic fit imposing energy momentum conservation of the 3 γ system. As shown in the following, the η mass value is insensitive to the calorimeter energy calibration and the systematic error on the measurement is dominated by the uniformity of the detector response. The decay channel $\phi \to \pi^0\gamma, \pi^0 \to \gamma\gamma$ is used as a cross-check of the method, comparing the π^0 mass obtained by this method with that reported in the PDG[1]. The result obtained is $m_\eta = 547.874 \pm 0.007_{\mathrm{stat.}} \pm 0.031_{\mathrm{syst.}}$and it is today best measurement of the η mass. The value is in agreement with the NA48[5] and in disagreement with the GEM measurement [6] and with the experiments performed before NA48.

1 Introduction

The η mass measurement has been performed using different techniques by several experiments in the history [1]. It was measured by hadron machines with different detectors and several production reactions.
The most recent measurements go back to 1974 at the Rutherford Laboratory. The experiment [2] used the reaction $\pi^- p \to n\eta$. The direction and the β of the n was accepted in a kinematic region such that the mass of the neutral system could be determined by measuring the momentum of the π^- beam. The value obtained is $m_\eta = 547.45 \pm 0.25$ MeV/c^2.

A later measurement at SATURNE [3] used the determination of the threshold of the reaction $d\,p \to {}^3He\,\eta$. The beam momentum at threshold was used to determine the η mass, and two reactions were needed in order to calibrate the beam momentum $d\,p \rightarrow {}^3He\,\pi^+$ and $d\,p \rightarrow p\,d$, they measured $m_\eta = 547.30 \pm 0.15$ MeV/c^2.

Again with threshold determination of the reaction $\gamma p \rightarrow \eta p$ the η mass was measured at the MAMI[4] accelerator with the TAPS experiment. The photons were produced by the bremsstrahlung of electrons on a radiator foil and the energy measured as the difference between the going out electron, measured in a spectrometer, and the incoming electron energy. The measurement relies on the determination of the η production threshold. They measured $m_\eta = (547.12 \pm 0.06 \pm 0.25) MeV/c^2$.

The first precise measurement was performed by the NA48 collaboration using the $\eta \rightarrow 3\pi^0$ decay. Small sensitivity to the calorimeter absolute scale was shown because the invariant mass was built using mainly the positions of the clusters and referenced to the π^0 mass. Cross-checks were done using the $\eta \rightarrow \gamma\gamma$ decay and the same technique was used to determine the K_L mass from $K_L \rightarrow 3\pi^0$.

The NA48 experiment measured $m_\eta = 547.843 \pm 0.030 \pm 0.041$[5], a value that is 0.6 MeV/c^2 higher than the average of the previous measurements and more than 5σ away.

This situation triggered a new high precision measurement at the COSY facility by the GEM collaboration[6]. In this case, a missing mass technique was used to determine the η mass in the reaction $p + d \rightarrow {}^3He + \eta$. The spectrometer was calibrated using two other reactions. The final result is $m_\eta = 547.311 \pm 0.028_{\mathrm{stat}} \pm 0.032_{\mathrm{syst}}$ MeV/c^2.

This last measurement is in disagreement with the NA48 measurement and agrees with the old experiments. The present situation is summarized in fig. 1.

The average of all the measurements but NA48 is 547.298 ± 0.040 MeV/c^2. The discrepancy with NA48 is at 8 σ. For this reason KLOE has performed a measurement of the η mass in order to clarify the situation.

The purpose of this work is to provide the best measurement of the η mass, in order to clarify the experimental situation.

2 The method.

At KLOE a large number of η mesons is produced through the electromagnetic decay $\phi \rightarrow \eta\gamma$. One of the main decay mode of the η meson is $\eta \rightarrow \gamma\gamma$ with $Br(\eta \rightarrow \gamma\gamma) \cdot Br(\phi \rightarrow \eta\gamma) = 0.5\%$. The decay chain produces three clusters in the calorimeter.

In order to achieve a precision of 5×10^{-5} level, needed to reach the target of the work, we cannot use directly the calorimeter energy measurement due to the uncertainty in the calorimeter energy calibration.

The method presented in this memo is based on the fact that in a 3 photons system the energy momentum conservation imposes 4 constraints to the photon kinematics.

The kinematics of the system is determined by the energies of the 3 photons

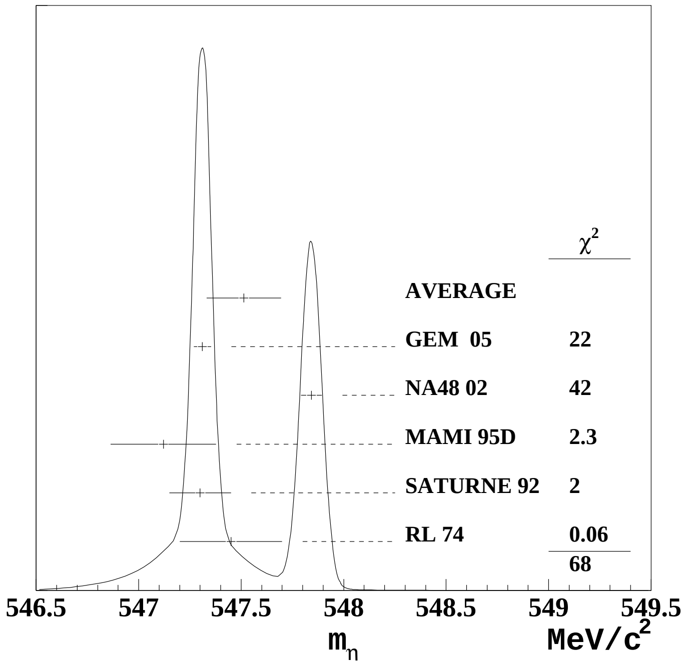

Figure 1: η mass measurement, see text for the references. The continuous line and the average has been computed using the PDG procedure [1], page 14.

and by the 6 angles of emission. Using the 4 energy-momentum constraints, it is in principle possible to express the energies as a function of the 6 angles. This work is done by a kinematic fit that imposes the following constraints:

- The total quadrimomentum of the three photons: P_x, P_y, P_z, E_{tot}[1];
- $t_i - r_i/c = 0$ for each cluster i, where r_i is the distance of the clusters from the interaction point (i.p. in the following) and t_i is the measured cluster time.

The procedure used for the fit is the same used for the $\eta \to 3\gamma$ upper limit determination [7]. The total quadrimomentum is determined by the **BMOM**, **BPOS** algorithm [8] that studies the Bhabha events to determine the mean vertex position X_v, Y_v, Z_v and the ϕ momentum.

The constraints on the time of the clusters improve the resolution on the z coordinate of the cluster and therefore on the angle of the photons. This is shown in fig. 2 for a MC simulation of the $\phi \to \eta\gamma$ events. This distribution has been obtained by evaluating the difference between the reconstructed z of the cluster and the z position of the extrapolated photons at the cluster centroid starting from the i.p. An improvement of about 40% on the resolution is obtained by the fit.

[1]In the KLOE refernce system the z axis is the bisectrix of the angle of the beams, the y axis is going upward and the x axis complete a left-handed system

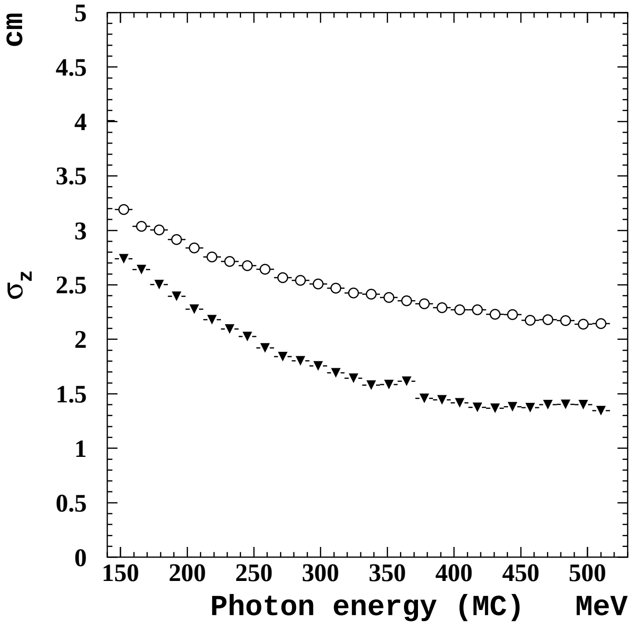

Figure 2: Resolution on the z coordinate of the photons as a function of the true MC energy. Open circles are before the kinematic fit; full triangles are after the kinematic fit with the $t - r/c$ constraint.

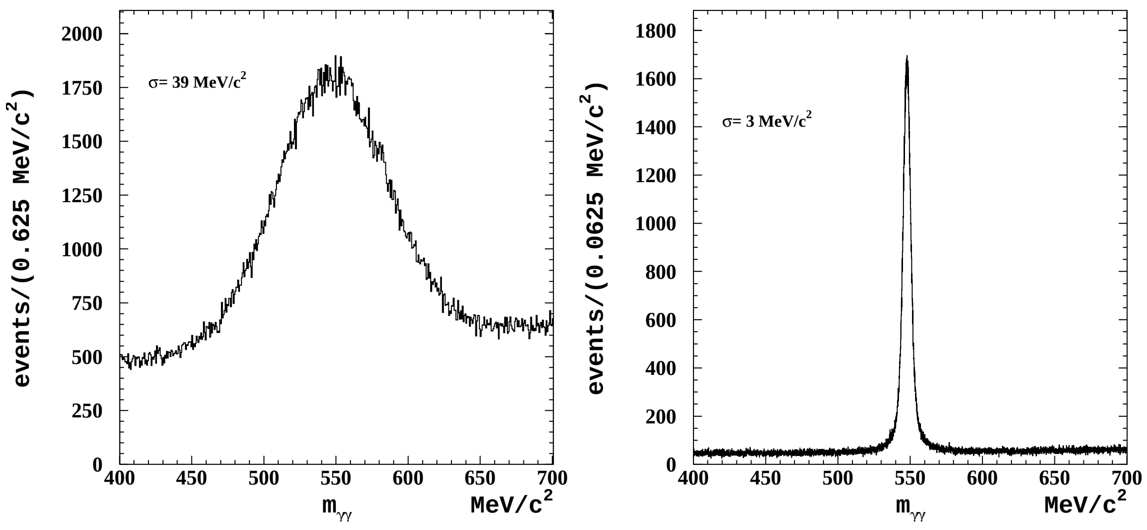

Figure 3: **(left)** m_η distribution built before using the energies in input to the kinematic fit, **(right)** the same after the kinematic fit.

The effect of the kinematic fit can be appreciated in fig. 3. On the left side the combinatorial $m_{\gamma\gamma}$ is plotted using the photon energies in input to the kinematic fit, while on the right using the output of the kinematic fit. In both case a $\chi^2 < 100$ is required to reject the main part of the background. The huge improvement in the mass resolution is evident.

3 Signal selection

The selection of the signal is very simple. With high statistics we can require high quality events in order to reduce all systematic effects. After the usual FILFO and Event-classification filters [9] for the radiative stream, we require at least three clusters whose time and position is compatible with the photon velocity:

$$|t - r/c| < min(5\sigma_t, 2\text{ns}) \tag{1}$$

where σ_t is parametrized according to the formula:

$$\sigma_t = \frac{54\text{ps}}{\sqrt{E(\text{GeV})}} \oplus 140\text{ps}$$

with an angle θ_γ: $50° < \theta_\gamma < 130°$.

Let's indicate with N_{pre} the number of clusters that survive this preselection. For each combination of three clusters of the total $\binom{N_{pre}}{3}$ we compute the sum of the

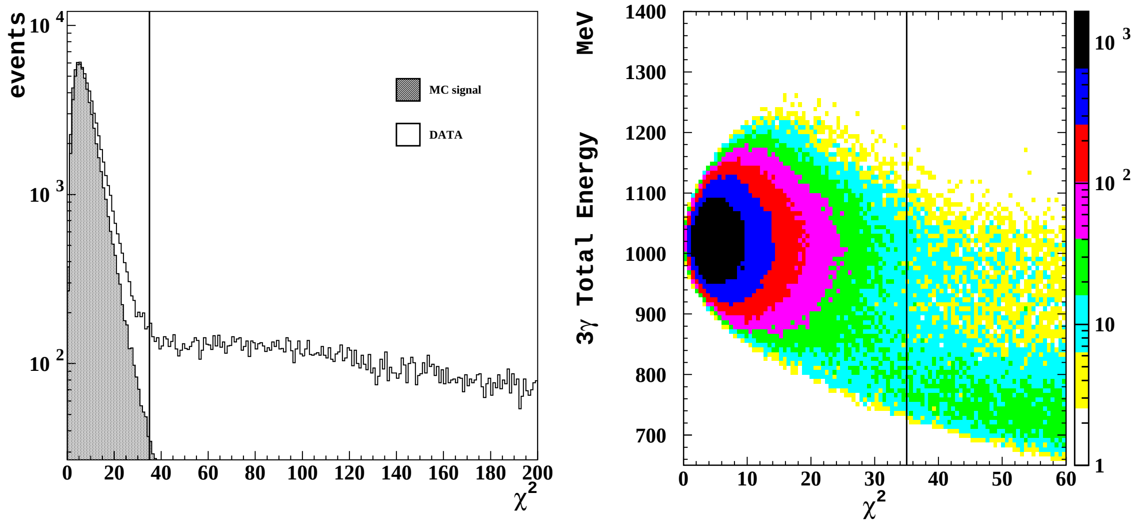

Figure 4: **(left)** χ^2 distribution for data and MC (3γ sample), the cut used is shown; **(right)** Scatter plot of E_{tot} versus χ^2 on the DATA sample. The line shown refers to the cut used to select a clean sample of $\eta \to \gamma\gamma$ continuous line, and $\pi^0 \to \gamma\gamma$ dashed line.

energies of the clusters E_{tot}, and we select the combinations with $E_{\mathrm{tot}} > 650\mathrm{MeV}$[2]. To these the kinematic fit procedure is applied.

The selected combinations are sorted according to the χ^2 of the fit and the combination with the smallest χ^2 is retained as an effective three photons event.

The cut $\chi^2 < 35$ rejects background with number of photons greater than 3,$\phi \to \eta\gamma, \eta \to 3\pi^0$, $\phi \to f_0\gamma, f_0 \to \pi^0\pi^0$, and $\phi \to a_0\gamma, a_0 \to \eta\pi^0$, or signal whith one photon lost and one from accidental machine background mimiking a photon cluster .

In fig. 4 (left) the χ^2 distribution of the DATA and of the MC events with 3γ ($\phi \to \pi^0\gamma$, $\phi \to \eta\gamma$) is shown together with the chosen cut. The signal is practically unaffected by the cut.

In fig. 4 (right) the scatter plot of E_{tot} as a function of the χ^2 is shown. It is evident that, given the cut $\chi^2 < 35$ (shown in the figure), the cut at 650 MeV is completely ineffective on the signal selection so that the systematics due to this last cut can be neglected.

In order to identify the signal and the several background sources we sort the 3 γs according to their energies $E_1 < E_2 < E_3$, and we build the Dalitz plot using the the invariant masses of the pairs 1-2 (m^2_{12}) and 1-3 (m^2_{13}). In fig. 5 these plots are shown for the data before and after the cut on the χ^2. The vertical band between 0 and 0.01 GeV^2 are the $\phi \to \pi^0\gamma$ events while the vertical line around 0.3 GeV^2 and

[2] The cut is applied to reduce the number of combinations on which the kinematic fit works, in order to save cpu time.

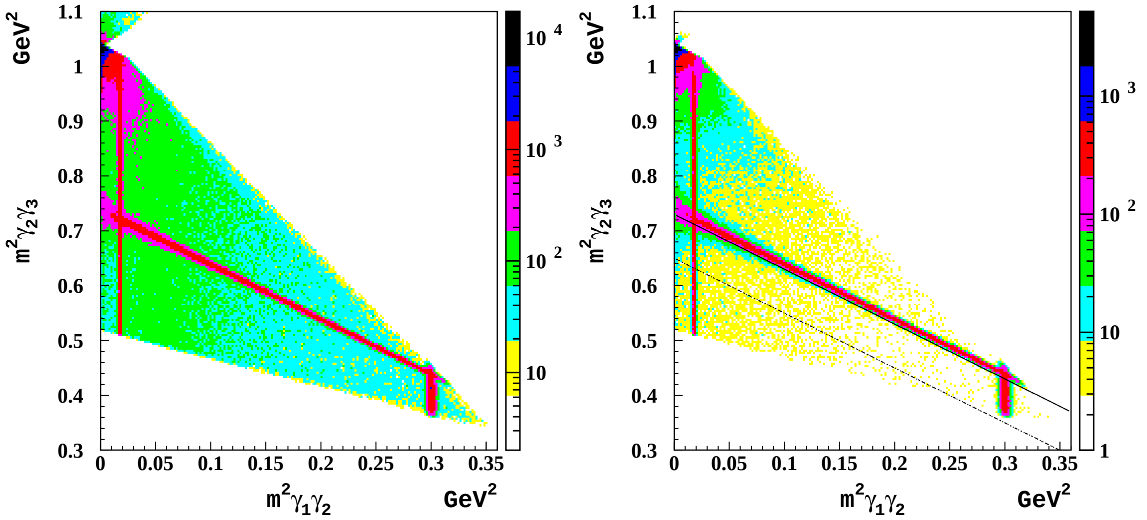

Figure 5: Dalitz plot distributions before (left) and after (right) the application of the $\chi^2 < 35$ cut. The continuous line is the cut applied to select $\eta\gamma$ events while the dashed line cut selects $\pi^0\gamma$ events.

the oblique line corresponds to the $\phi \to \eta\gamma$ events.

The $m_{\gamma1\gamma2}$ variable is plot in fig. 6 left. Two very narrow peaks are visible, the peak at the π^0 mass, due to the $\phi \to \pi^0\gamma$,$\pi^0 \to \gamma\gamma$ and the peak at the η mass coming from the decay chain $\phi \to \eta\gamma$,$\eta \to \gamma\gamma$. Under both peaks there is a large background. In the case of the η it is only due to the combinatorial background, that is when the photons 1-2 don't come both from the η decay but one of them from the ϕ decay. This can be easily deduced by looking at fig. 5. In fact being

$$m^2_{12} + m^2_{13} + m^2_{13} = m^2_\phi,$$

the line that crosses the center of the histogram is given by events in which the photons 1-3 come from the η decay. In the π^0 case there is not misidentification background because the photons coming from the π^0 are always the least energetic ones. In the π^0 case the background is given by the $\eta \to 2\gamma$ sample and by the $e^+e^- \to \gamma\gamma$ with an accidental cluster. These events are concentrated in the upper part of the Dalitz plot.

The uncertainty on the background shape and the correlation between the background parameters and the central value of the peak could spoil the precision of the measurement. For this reason it is important to clean the sample as much as possible and we perform background rejection using the following cuts:

$$\begin{aligned} \eta : m^2_{23} &< 0.73 - m^2_{12} \quad \mathrm{GeV}^2 \\ \pi^0 : m^2_{23} &< 0.65 - m^2_{12} \quad \mathrm{GeV}^2 \end{aligned}$$

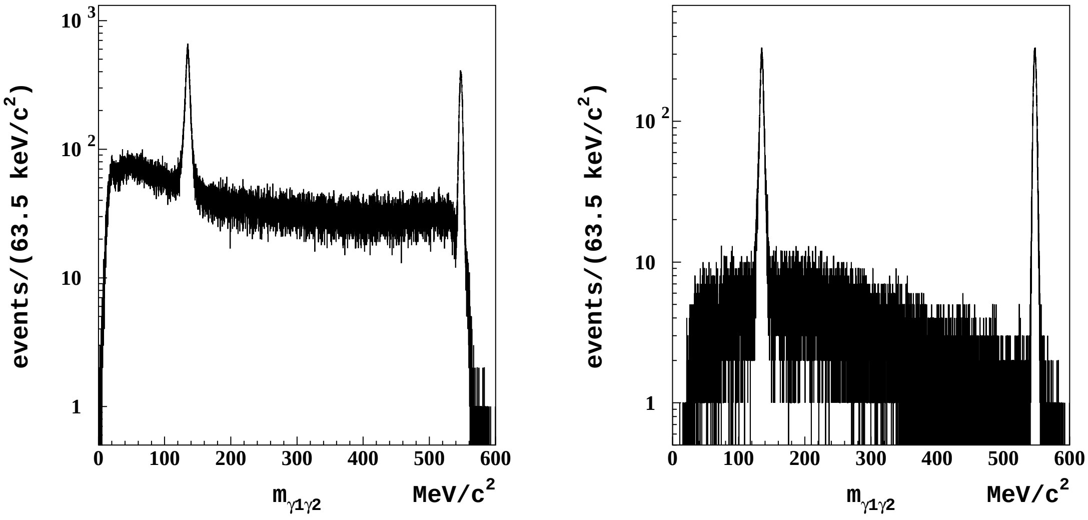

Figure 6: Invariant mass distribution of the least energetic photons $m_{\gamma_1\gamma_2}$.

fit results					
	χ^2/n.d.f	C.L.	m (MeV)	σ_1 (MeV)	σ_2 (MeV)
η	154/161	57 %	547.710 ± 0.014	2.14 ± 0.012	-
π^0	255/257	43 %	134.94 ± 0.02	1.78 ± 0.05	4.07 ± 0.19

Table 1: Fit parameters for the π^0 and η mass distribution. In the π^0 case the sigma of the two Gaussians are shown.

In fig. 6 the distribution of $m_{\gamma1\gamma2}$ is shown before (left) and after (right) the cut indicated with the continuous line in fig. 5. To determine the π^0 mass a stronger cut is needed in order to reduce the background at an optimum level (fig. 7), it is shown with the dashed line in fig. 5 (right).

The peak at the η mass value of fig. 6 has been fitted with a Gaussian distribution using a χ^2 minimization procedure performed with the MINUIT package. The result of the fit is shown in fig. 8 for 60 pb^{-1} in the 2001 data. A double Gaussian distribution is needed to reproduce the π^0 shape. The result of the fit are given in tab. 1. It is possible to see that the statistical error using 60 pb^{-1} of data is about 14 keV (3×10^{-5}). The high precision of the measurement implies the need for a careful study of all systematic effects that could spoil this level of precision.

4 Systematic error evaluation.

Several sources of systematic error have been studied. The considered effects are: uncertainty in calorimeter energy calibration, non linearity in the energy response,

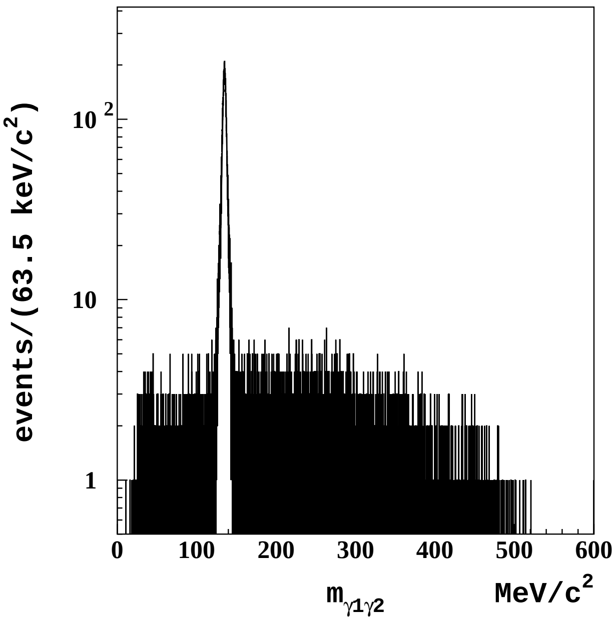

Figure 7: $m_{\gamma 1 \gamma 2}$ distribution for the π^0 selection.

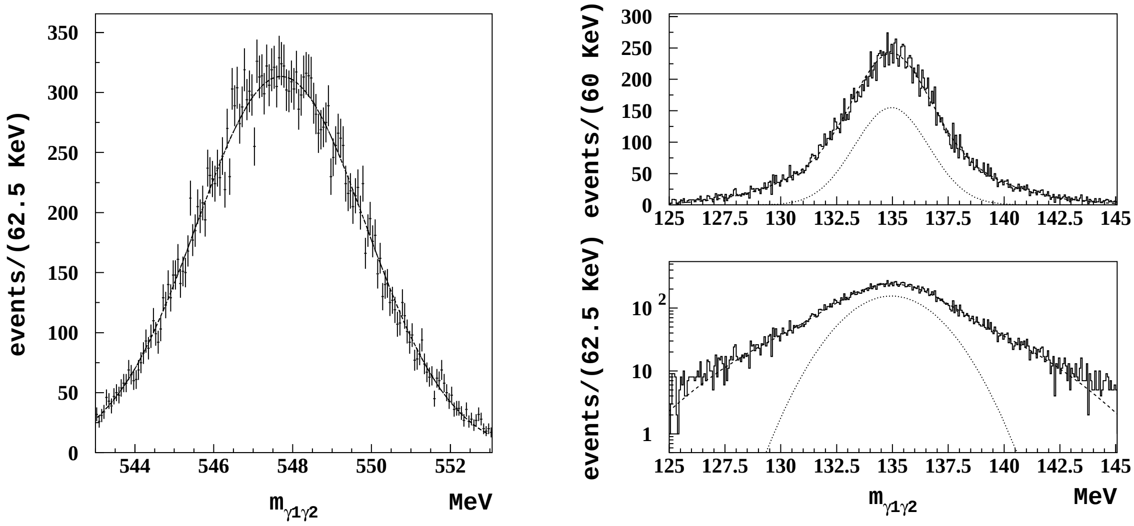

Figure 8: Invariant mass distribution for the $\eta \to \gamma\gamma$ decay (left) and for the $\pi^0 \to \gamma\gamma$ decay (right). The fitted function are shown. The small Gaussian in the π^0 case is the core Gaussian.

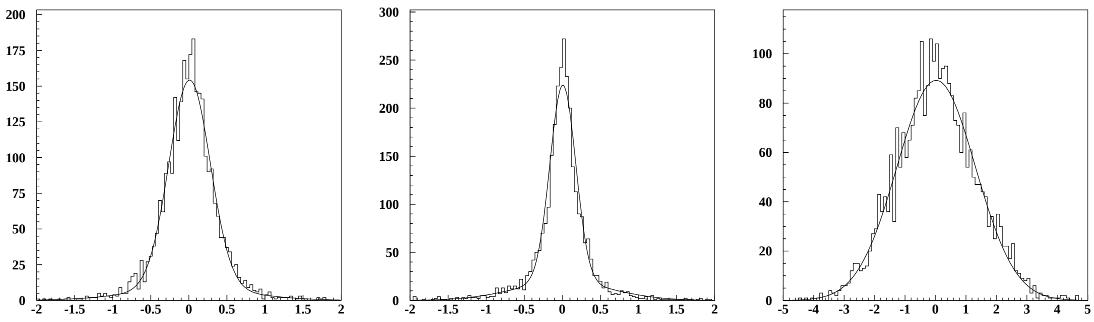

Figure 9: From left to right: $(X_{\pi\pi\gamma} - X_{BPOS})$, $(Y_{\pi\ \pi\gamma} - Y_{BPOS})$, $(Z_{\pi\pi\gamma} - Z_{BPOS})$.

disuniformity in the angular response in the azimuthal and polar angle, knowledge of the interaction point position, global misalignment between the Drift Chamber and the calorimeter, knowledge of $\sqrt{s}$, effect of the χ^2 cut , the Dalitz plot cut and Initial State Radiation effects. To evaluate some of these systematic effects we have used the $\pi^+\pi^-\gamma$ sample selected for the hadronic cross section measurement at large angle. This sample is used to estimate systematics on the determination of the vertex position, the calibration of the energy E and non-linearity, the misalignment between the Drift Chamber and the calorimeter.

4.1 Vertex position.

The vertex position is determined run by run by using Bhabha events. To evaluate a systematic error on this measurement we compare it with the vertex position reconstructed in the $\pi^+\ \pi^-\ \gamma$ events using the $\pi^+\pi^-$ vertex. The data set has been divided into groups of runs with the same integrated luminosity equal to 2 pb^{-1} for the 2001 and 0.5 pb^{-1} for 2002; for each group of runs the distributions of the quantities $(X_{\pi\pi\gamma} - X_{BPOS})$, $(Y_{\pi\ \pi\gamma} - Y_{BPOS})$, $(Z_{\pi\pi\gamma} - Z_{BPOS})$ are fit with the sum of two Gaussians with the same mean. The value of the mean should be zero if any not common systematic displacement between the Bhabha and the $\pi^+\pi^-\gamma$ sample is seen. The distribution of these 3 variables are shown for a given run range in fig. 9.

In fig. 10 we show the mean as a function of the run number at the beginning of each run group. The uncertainty due to the vertex position is estimated by evaluating the *rms* of these points respect to the expected value of zero. The rms is used as the systematic error on the interaction point position. In tab. 2 these errors are shown in the "rms i.p." column.

A possible common systematic between the $\pi\pi\gamma$ sample and the Bhabha can be due to a displacement, not corrected in the reconstruction, between the calorimeter and the DC. The i.p determined with the charged tracks is in the drift chamber reference frame, while the reconstructed photon positions are in the calorimeter reference

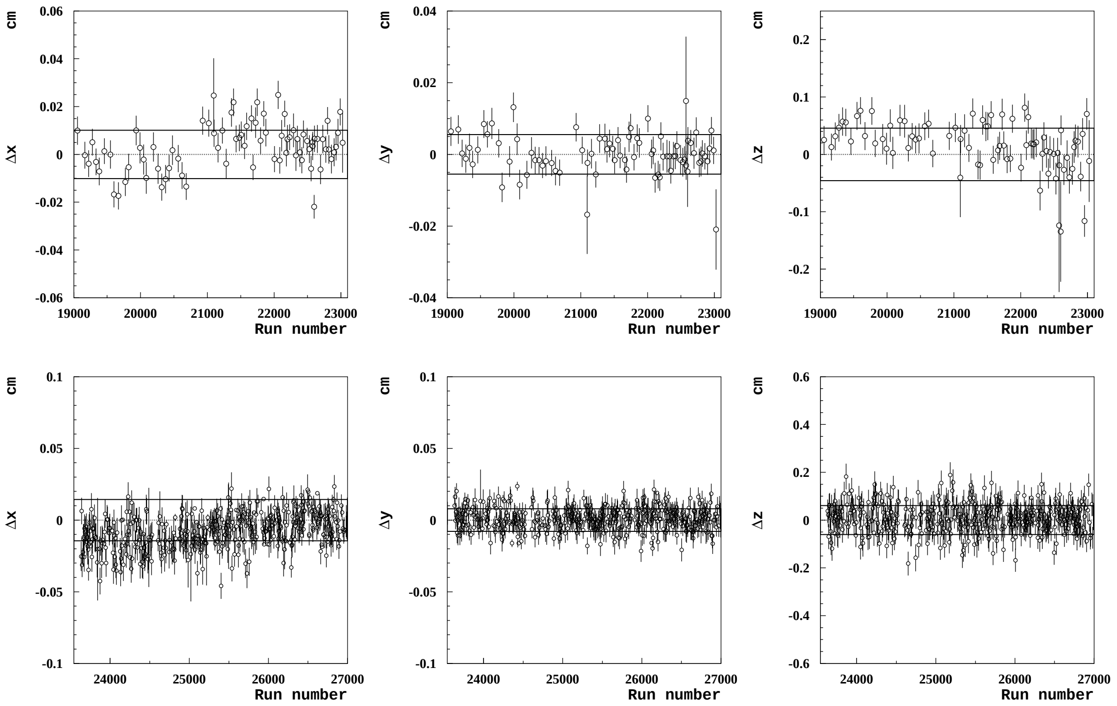

Figure 10: Vertex position difference between the $\pi^+\pi^-$ vertex and the $BPOS$ value. **Top** 2001 DATA, **bottom** 2002 DATA.

Systematic due to the vertex position (cm).							
	2001			2002			
coord.	rms i.p	DC-calo al. π^+	DC-calo al. π^-	rms i.p	DC-calo al. π^+	DC-calo al. π^-	tot. syst.
x	0.010	0.04	0.034	0.014	0.062	0.056	0.056
y	0.006	0.12	0.08	0.008	0.13	0.088	0.088
z	0.046	0.16	0.17	0.061	0.22	0.28	0.22

Table 2: Corrections to the vertex position and associated systematic error.

	m_η ($\times 10^{-6}$)	m_π ($\times 10^{-6}$)	m_η/m_π ($\times 10^{-6}$)
V_X	1.8	15	15
V_Y	7	22	27
V_Z	4	37	35
overall	8	45	47

Table 3: Fractional systematic error coming from the knowledge of the position of the vertex. The overall values is obtained summing in quadrature the individual contributes.

frame. In order to check the DC-calorimeter alignment, we use the extrapolation of the tracks of the $\pi^+\pi^-\gamma$ sample to the calorimeter. The tracks are extrapolated from the vertex to the calorimeter assuming a constant magnetic field of $0.5188T$ along the z direction. The point of closest approach to the cluster centroid is computed, where the cluster is that associated by the standard track to cluster algorithm. Any displacement between the DC and the barrel can be evaluated by studying the distribution of the residuals $X_{extr} - X_{clu}$, $Y_{extr} - Y_{clu}$, $Z_{extr} - Z_{clu}$. The average of the residuals on several groups of runs is plotted as a function of the first run of the period in fig. 12. The calorimeter is well centered along the x coordinate while it is shifted of about 1 mm along the y coordinate. The z coordinate varies as a function of the run number and this is due to possible miscalibration of the cluster times. The systematic error is evaluated as the standard deviation with respect to the expected value, 0, of all the distributions shown in the plot. The values are reported in tab. 2.
Both the uncertainty on the vertex position and on the displacement between the calorimeter and the drift chamber have the same effect on the measurement. They change the angle between the two photons coming from the η decay and so they have to be accounted together. The two effects are completely uncorrelated, so we sum in quadrature the errors. We take the smallest value between the rms' obtained with the π^+ and the π^- track. in fact any discrepancy can only be due to the way with which the particles interact in the calorimeter or to the constant B field approximation, that can enlarge the *rms* bringing to an overestimate of the uncertainty on the misalignment but never underestimating it.

To be conservative for the DC-Calo alignment systematic we take the values of 2002 because the uncertainty is higher. The overall error is shown in the last column of tab. 2. To evaluate the effect of these uncertainties on the value of the η mass we proceed in the following way: we apply run by run a systematic shift of $\pm$ 1 σ on the vertex position reported in tab. 2. We repeat the analysis and extract the value of the η mass. The difference with respect to the central value as a function of the shift of the vertex position is shown in fig. 13, 14 and 15. From this figure we extract the contributes to the systematic error for the mass of the π^0, the η and the ratio m_{π^0}/m_η. The value obtained are shown in tab. 3

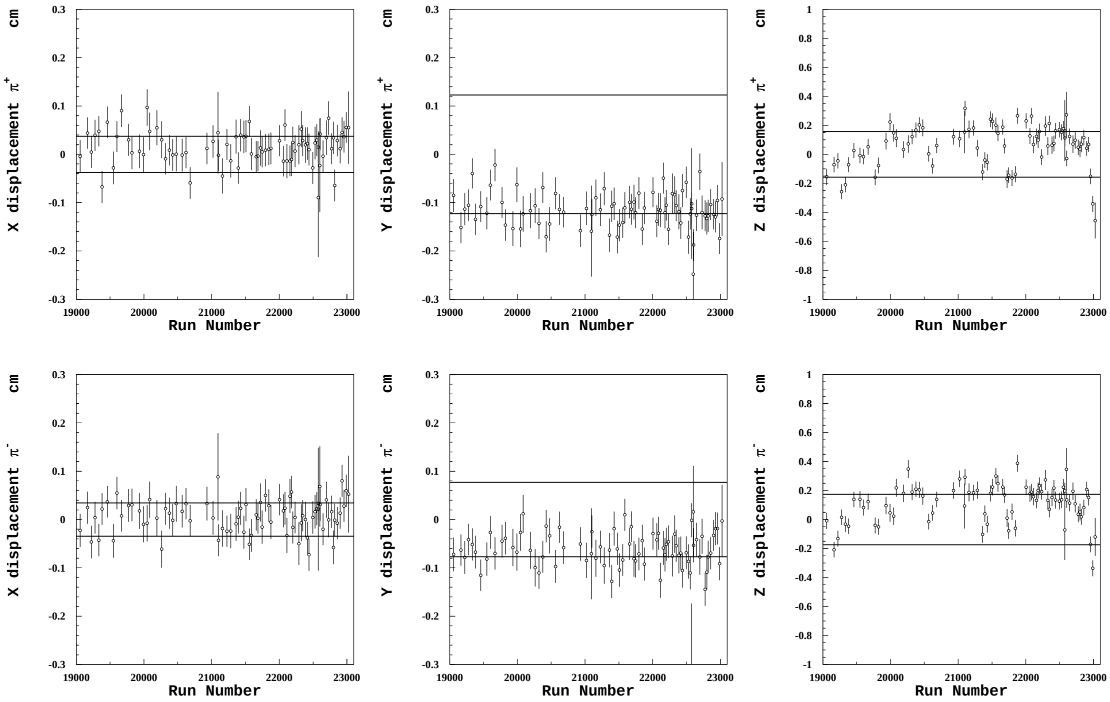

Figure 11: Mean of the residuals of the extrapolated track position with respect to the cluster centroid for π^+ and π^- in the year 2001.

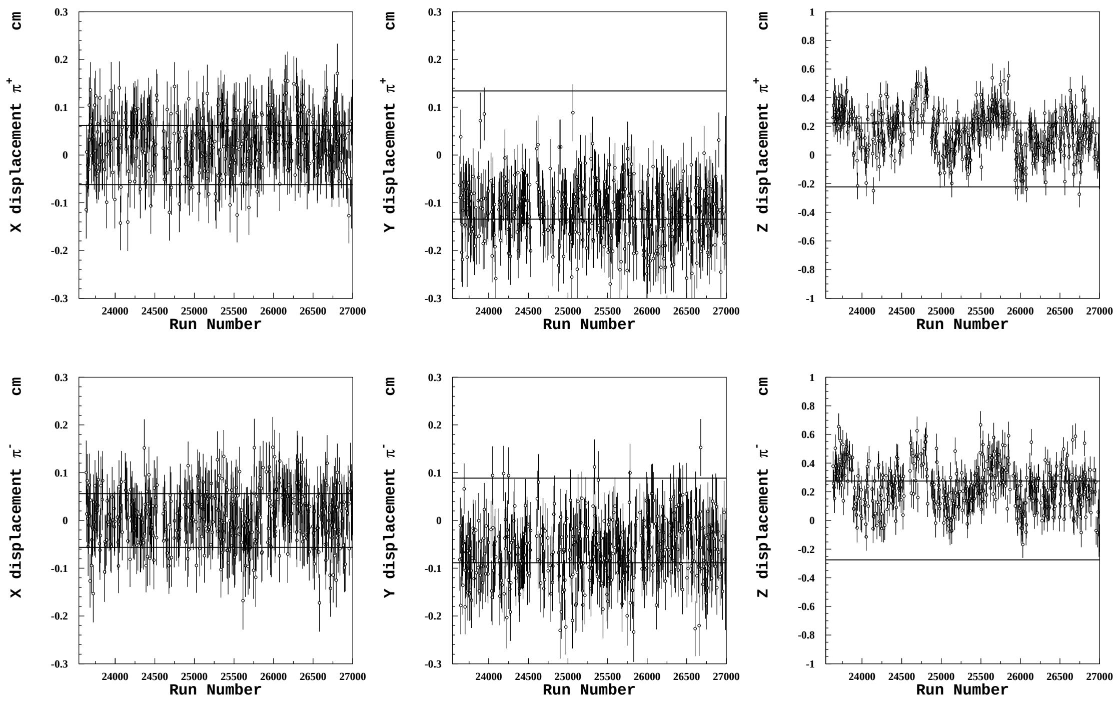

Figure 12: Mean of the residuals of the extrapolated track position respect the cluster centroid for π^+ and π^- in the year 2002.

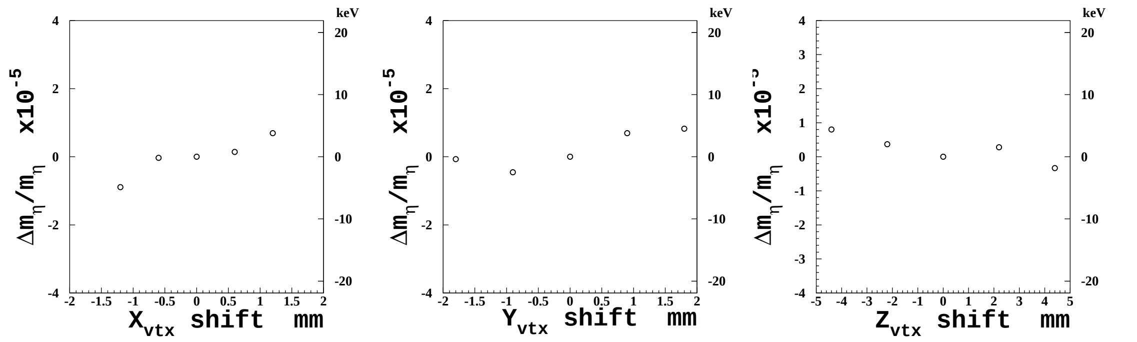

Figure 13: The η mass fractional shift as a function of the vertex position shift.

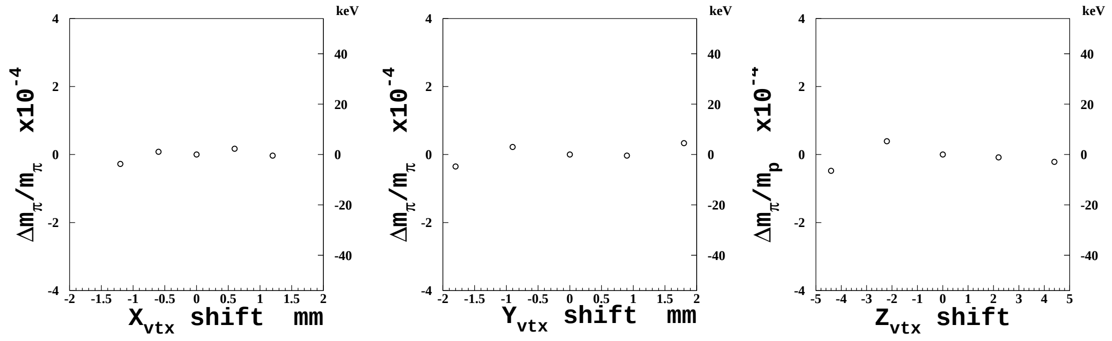

Figure 14: The π^0 mass fractional shift as a function of the vertex position shift.

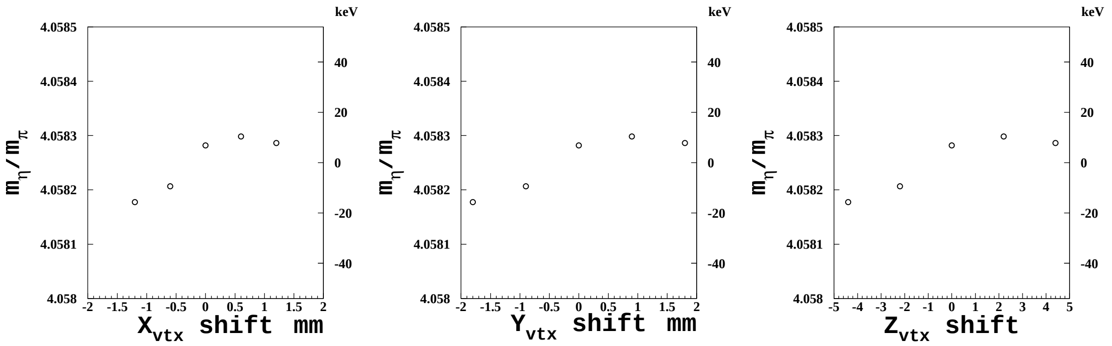

Figure 15: The $m(\eta)/m(\pi^0)$ ratio as a function of the vertex position shift.

	m_η ($\times10^{-6}$)	m_π ($\times10^{-6}$)	m_η/m_π ($\times10^{-6}$)
calibration constants	7	7	14
linearity deviation	7	81	76

Table 4: Fractional systematic error coming from the knowledge of the calorimeter energy response.

4.2 Energy response.

To estimate the systematic error on the knowledge of the linearity of the energy response of the calorimeter, we have used the $\pi^+\pi^-\gamma$ events as a control sample. To this purpose we evaluate the missing energy from the $\sqrt{s}$ and the two charged pions momenta and we compare it with the energy of the prompt clusters in the calorimeter [a cluster is called "prompt" if it satisfies the relation (1)]. From this study the calibration constant of the calorimeter result to be known at 1% level while the linearity of the response is better than 2% in the entire energy range. These results are in agreement with the studies performed using the $e^+e^- \to e^+e^-\gamma$ [9].

The variation of the η mass obtained applying the estimated miscalibration and linearity deviation are shown in tab. 4.

4.3 Calorimeter response uniformity.

Other systematic effects can be due to the disuniformity of the calorimeter response as a function of the cluster position. To evaluate the systematic uncertainty due to these dis-homogeneities we evaluate the η mass as a function of the azimuthal and polar angle of a vector orthogonal to the 3γ plane in the ϕ rest frame.

The vector is determined using all three versors of the 3γ $(\hat{v}_1, \hat{v}_2, \hat{v}_3)$ sorted according to their energies. Due to the cut on the Dalitz plot the versor $\hat{v}_3$ is the direction of the photon from the ϕ decay. The cross vectors:

$$\hat{c}_1 = \frac{\hat{v}_3 \times \hat{v}_1}{|\hat{v}_3 \times \hat{v}_1|} \quad \hat{c}_2 = \frac{\hat{v}_2 \times \hat{v}_3}{|\hat{v}_2 \times \hat{v}_3|}$$

are computed. They should have the same direction and versus within the measurement uncertainties. So we take the average $(\hat{c}_1 + \hat{c}_2)/(|\hat{c}_1| + |\hat{c}_2|)$. The value of the η mass as a function of the angle ϕ between the projection of the vector in the $x-y$ plane and the y-axis (fig. 16) is shown in fig. 17, left. The rms of the data points is taken as systematic error on m_η. The same plot for the angle θ, complementary to the angle between the versor and the z axis, is shown in fig. 17, right. The missing points in the center of the figure are due to the angular cut on the photons $50° < \theta_\gamma < 130°$. The rms of these points is again taken as systematic error. The systematic error on the masses obtained are reported in tab. 5.

	m_η (keV)	m_π (keV)	m_η/m_π
azimuthal uniformity	15	12	3.7×10^{-4}
polar uniformity	10	44	1.2×10^{-3}

Table 5: Systematic error coming from the dis-homogeneous response of the calorimeter.

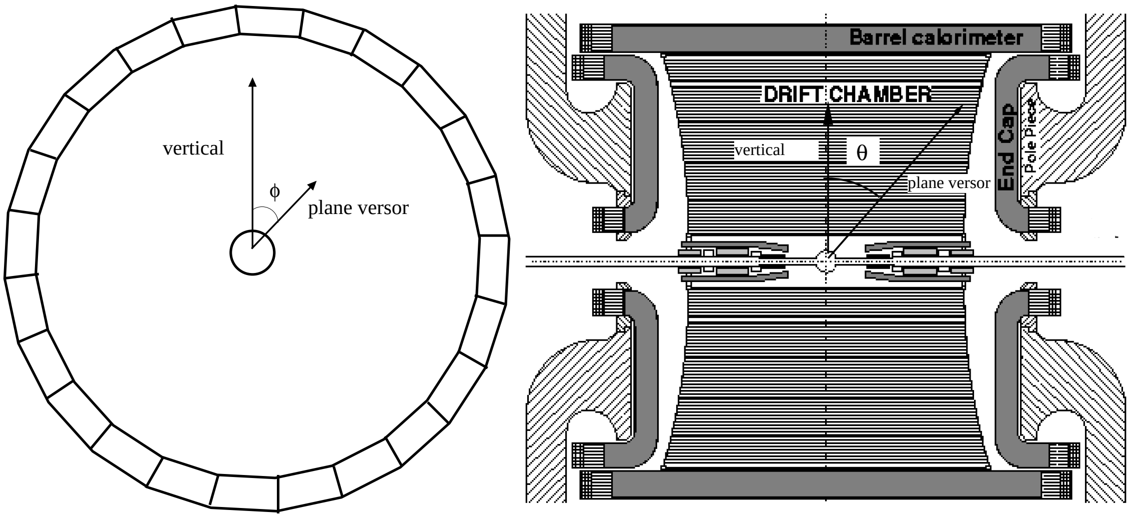

Figure 16: Illustration of the azimuthal and polar angle definition.

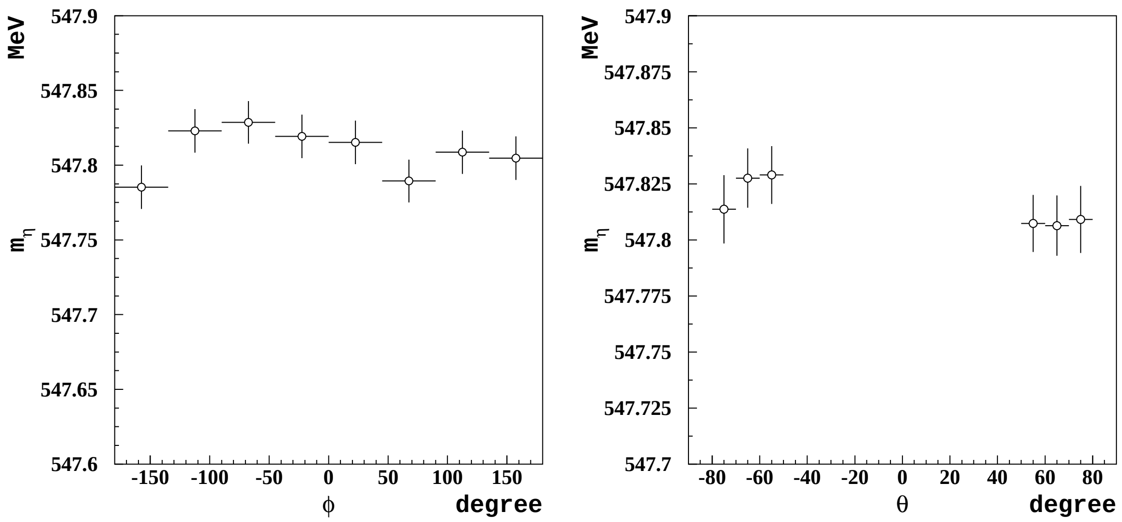

Figure 17: **left** m_η as a function of the azimuthal angle; **right** m_η as a function of the polar angle.

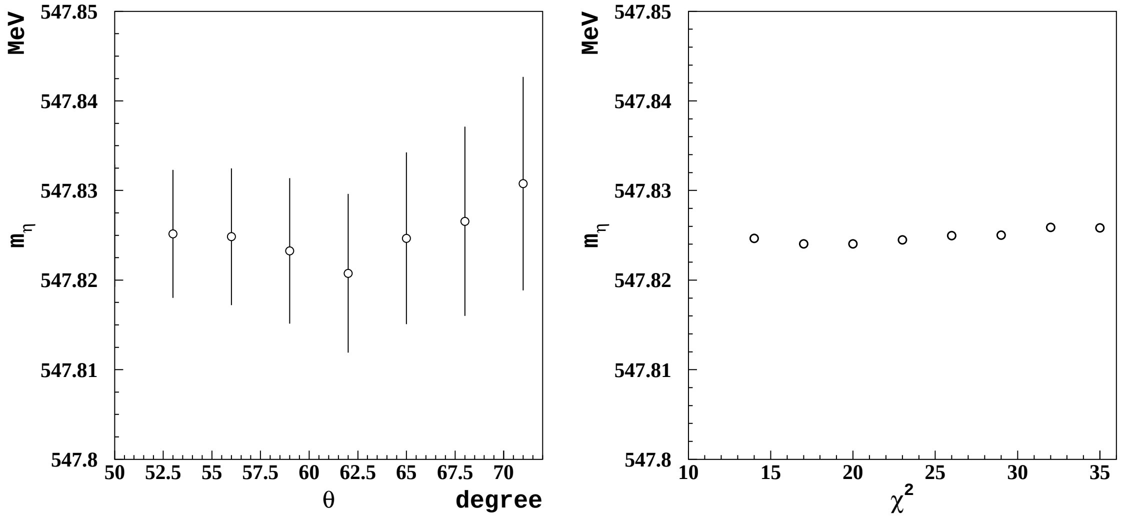

Figure 18: **left** η mass as a function of the angular cut, **right** η mass as a function of the χ^2 cut.

	m_η (keV)	m_π (keV)	m_η/m_π
χ^2 cut	0.7	4	1.3×10^{-4}

Table 6: Systematic error coming from the χ^2 cut.

As a cross-check of the above residual calorimeter disuniformity, we varied the angular cut on the photons between 50° and 70° and we recomputed the mass. The plot is shown in fig. 18.

The rms of the point distribution is 3 keV, smaller than that obtained before. In the π^0 case an angular dependence is seen bringing to a systematic error of 48 keV, in agreement with that estimated by the polar uniformity checking while an effect of 1.4×10^{-3} is seen on the ratio of the masses.

The dependence of the measured value from the choice of the χ^2 cut value has been studied using more hard χ^2 cut. In fact an harder χ^2 cut cleans the sample from an eventual residual background and no variation is expected on the value of the measured mass. An eventual shift has to be considered as a systematic effect. From fig. 18 the value of the mass as a function of the cut has been shown. The systematic due to this cut is shown in tab. 6.

4.4 Dalitz plot cut.

Another important systematic error comes from the choice of the cut in the Dalitz plot. This cut is completely arbitrary. Due to the finite width of the mass distribution given by the detector angular and time resolution the projected mass

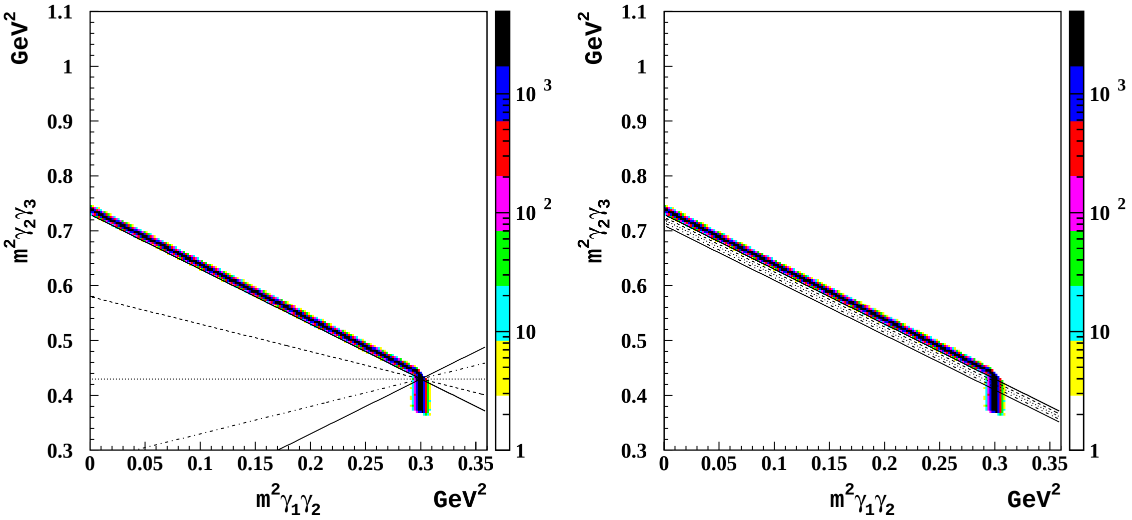

Figure 19: Different cut choices on the Dalitz plot. The band is the plot is produced by the toy MC.

Width of the m_η distribution.		
MeV	DATA	MC
σm_η	2.137 ± 0.012	2.514 ± 0.012
$\sigma_1 m_\pi$	1.78 ± 0.05	1.86 ± 0.10
$\sigma_2 m_\pi$	4.07 ± 0.19	3.53 ± 0.34

Table 7: Comparison between the width of the Gaussian peak for the π^0 and for the η mass distribution.

distribution is distorted by the cut. In fig. 19 we show two different ways to change the cut: on the left several slopes for the straight line cut, while on the right the cut is changed by a constant shift, drawing a parallel set of line on the plot. The η mass value as a function of this cut is shown in fig. 20.

One can easily see that this gives a variation of the order of 200 keV, enough to spoil the accuracy of this measurement. Anyway the effect is very easy to understand. It is just a geometric distortion of the distribution in the Dalitz plot shown in fig. 5. It is enough to use a Dalitz plot distribution whose points are distributed according a Gaussian with the σ equal to that of the data to predict the effect.

In fig. 22 the same distribution built with the MC sample has been shown.

As one can see in table 7 there is an important discrepancy between data and MC on the width of this distribution.

In particular the data distribution is narrower than MC distribution. For this reason we cannot use just the MC to predict the shifting effect and correct the value,

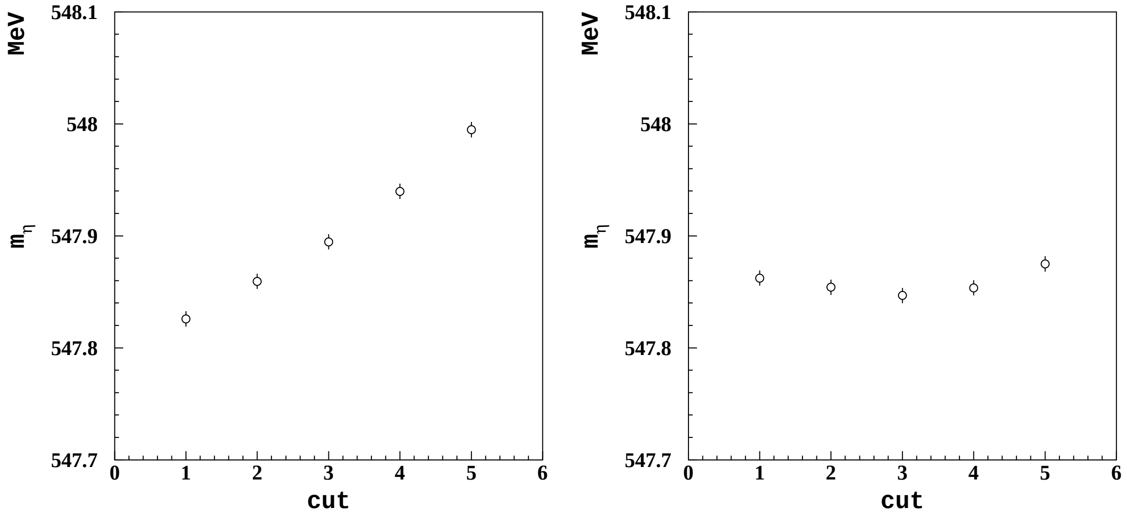

Figure 20: η mass variation as a function of the slope of the straight line cut on the Dalitz plot.

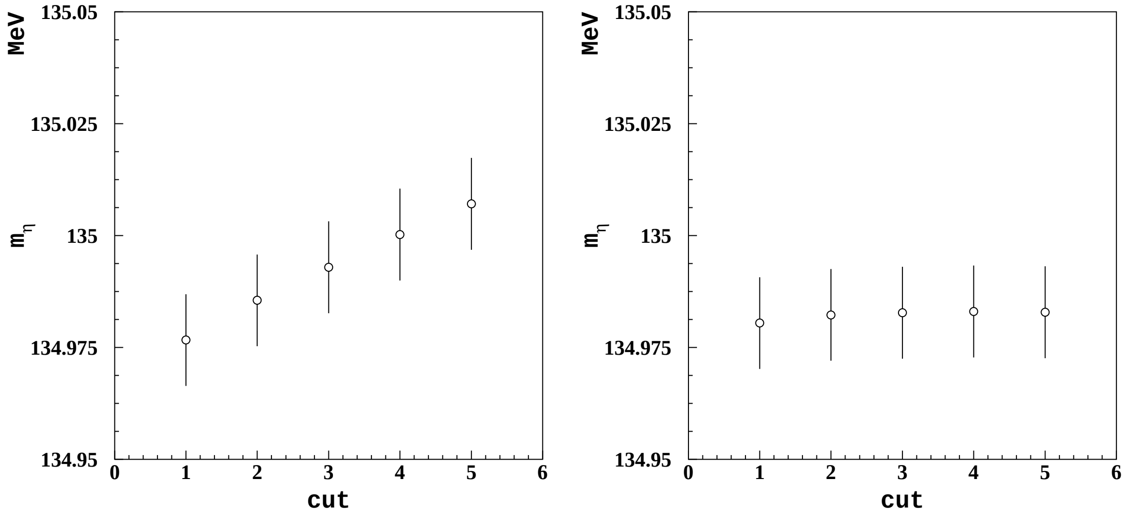

Figure 21: π^0 mass variation as a function of the slope of the straight line cut on the Dalitz plot.

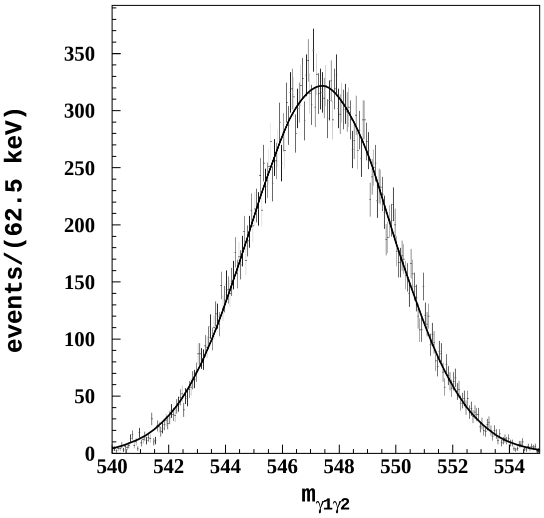

Figure 22: m_η distribution (MC).

Variation of m_η from the choice of the cut on the Dalitz plot.			
cut	MC ($m_\eta = 547.78$ MeV/c^2)	data	data corrected
0.73 -x	547.744 ± 0.001	547.826 ± 0.007	547.862
0.58 -0.5x	547.785 ± 0.001	547.859 ± 0.007	547.854
0.43	547.828 ± 0.001	547.895 ± 0.007	547.847
0.28+0.5x	547.866 ± 0.001	547.94 ± 0.007	547.854
0.13+x	547.900 ± 0.001	547.995 ± 0.007	547.875

Table 8: m_η values obtained for several choices of the slope of the cut.

furthermore being the data distribution narrower than the simulated, we cannot apply any smearing to the distribution to obtain a better data-MC agreement. Being the effect just linked to the width of the distribution we can evaluate the correction with a very simple toy MC. The MC generator is done simulating η meson decays with a Gaussian mass distribution whose width is the value obtained from the data. The values of the obtained mass for the several cuts are shown in tab. 8 together with the values obtained from data, the difference between the cut and the reference values is used to correct the data value.

The shift observed on the toy MC distribution is used to correct the data values. The corrected values are shown in the third column of the table. In fig. 20 (right) the mass values as a function of the cut are plotted for the corrected values. In the case of the constant shift, no predictable systematic effect due to the distortion of the distribution is seen, the eta mass values obtained as a function of the cut is

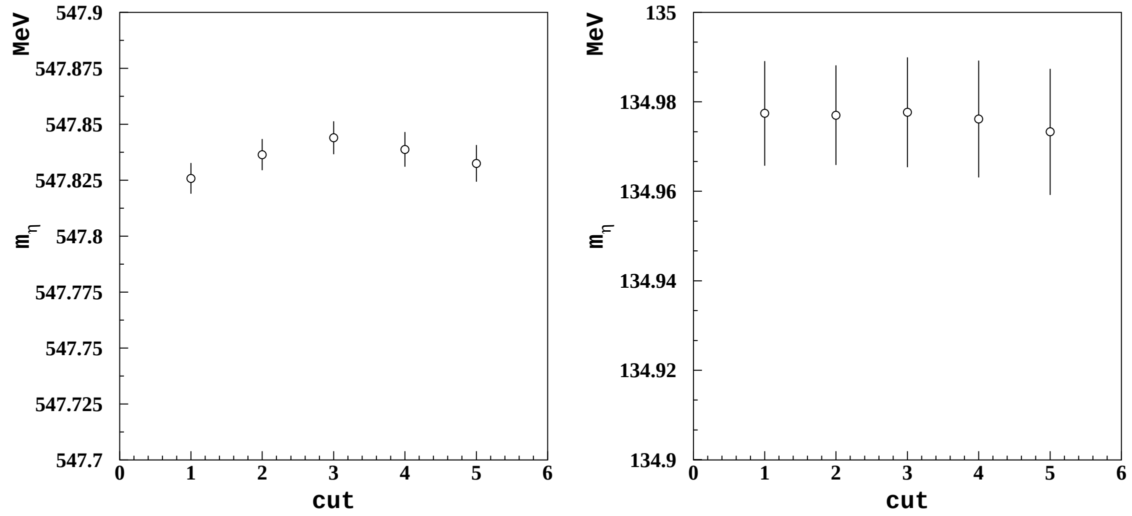

Figure 23: m_η and m_{π^0} values obtained for several choices of the constant in the Dalitz plot cut.

Systematic due to the Dalitz plot cut		
	syst. const	syst. slope
m_η	12 keV	12 keV
m_{π^0}	1.9 keV	4 keV
m_η/m_π	10×10^{-5}	15×10^{-5}

Table 9: Systematic due to the choice of the cut on the Dalitz plot.

shown in fig. 23. The same work done for the π^0 is shown in fig. 21 and fig. 23. The rms of this distribution is taken as systematic effect. The systematic errors for these cuts are shown in tab. 9.

4.5 $\sqrt{s}$ determination

The mass is very sensitive to the values used for $\sqrt{s}$. The dependence of the η and π^0 mass as a function of a shift on the real value of $\sqrt{s}$ is shown in fig. 24.

The correction follows the law:

$$\frac{m'_\eta}{m_\eta} = \frac{m'_{\pi^0}}{m_{\pi^0}} = \frac{\sqrt{s'}}{\sqrt{s}}$$

The $\sqrt{s}$ is determined from a fit to the Bhabha differential spectrum taking into account initial state radiation. For this reason, it is important to select data sample that are acquired in the most stable condition of the machine. During the 2001 and 2002 data taking, several runs were acquired in various conditions due to the

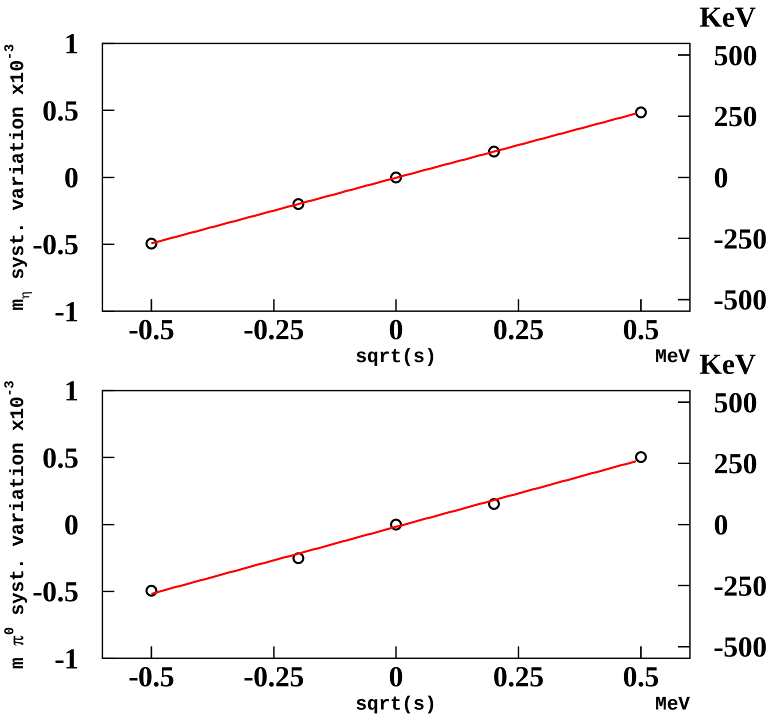

Figure 24: Behavior of the η and π^0 masses as a function of the $\sqrt{s}$.

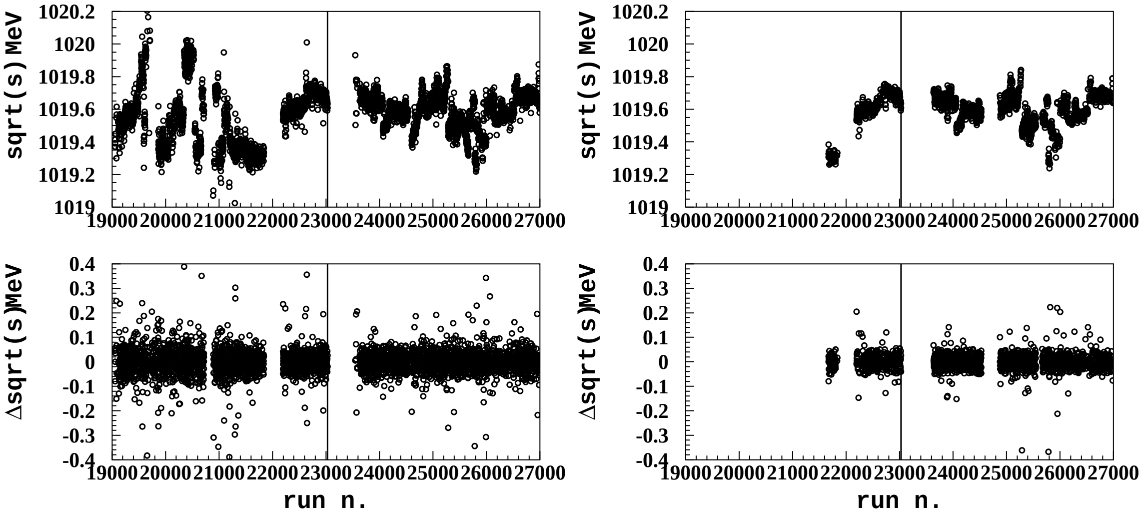

Figure 25: **left** all runs acquired in good trigger conditions and good time calibration, **right** Runs chosen for the data analysis; **top** $\sqrt{s}$ as a function of the run number, **bottom** difference in $\sqrt{s}$ between one run and the previous run for the whole sample of good runs. The vertical line separate the 2001 from 2002 data taking.

continuous changing of machine parameters in order to optimize the machine to reach higher luminosity. The result of this approach has been a big increase of the machine luminosity during the time but at the same time the acquisition, in some periods, of low quality data. This can be seen in fig. 25 where the value of the $\sqrt{s}$ has been plot as a function of the run number for the whole 2001 + 2002 data taking. Also some runs acquired with a bad trigger conditions or with wrong time calibration were rejected. In the figure we can see several jumps in the $\sqrt{s}$ value, and some period with very fast variation of the $\sqrt{s}$.

In order to keep the error on the parameters of this fit to a reasonable level ($<$ 60 keV) more than 100 nb^{-1} of data are needed. For this reason we discard all the runs whose collected luminosity is below $100nb^{-1}$. Moreover we reject all the runs where the measured $\sqrt{s}$ of two consecutive runs differs by more than 50 keV, this allows to reject runs in which the $\sqrt{s}$ determination algorithm failed for any reason. The same plot done using this reduced run sample is shown in figure 25.

The absolute scale of $\sqrt{s}$ has been derived using the ϕ line shape in the decay $\phi \to K_L K_S$ [10]. The ϕ mass from the ϕ line shape results 154 keV below the value measured by the CMD-2 collaboration [11]. This suggests to shift the value of the $\sqrt{s}$ by 154 keV up, assuming as systematic due to this correction the error on the ϕ mass measured by CMD-2 and the statistical error of our ϕ line shape measurement.

This gives:

$$\Delta\sqrt{s} = 154 \pm 11_{\text{KLOE stat.}} \pm 11_{\text{CMD-2 stat.}} \pm 32_{\text{CMD-2 syst.}} \quad \text{keV}$$

where the CMD-2 systematic error comes from the knowledge of the beam energies.

4.6 MC simulation.

In using standard MC tools we have found small problems in the simulation of the cluster position, the i.p position and time resolution. These very small effects are important for our analysis due to the high precision required. In order to overcome these problems we have used a toy MC generation.

This MC uses the standard simulation tool to simulate the production-decay process of the $\phi \to \eta\gamma, \eta \to \gamma\gamma$ and to track the photons up to the calorimeter surface, but the calorimeter response is simulated by smearing the conversion point position, the arrival time of the photons and their energies, sampling a gaussian distribution with the following σ's:

$$\sigma_x = \frac{3.4}{\sqrt{12}}\ \text{cm} \quad \sigma_y = \frac{2.81}{\sqrt{12}}\ \text{cm} \quad \sigma_z = \frac{0.9}{\sqrt{E(\text{GeV})}}\ \text{cm}$$

$$\sigma_t = \frac{54\text{ps}}{\sqrt{E\ (\text{GeV})}} \oplus 140\ \text{ps} \quad \frac{\sigma_E}{E} = \frac{0.057}{\sqrt{E(\text{GeV})}}$$

To have a good agreement we also simulated the luminous region along the z axis as a gaussian with $\sigma_{zl} = 1.95$ cm. The pulls of the z coordinate on DATA were not centered at zero, to restore the correct position a small alignment of 1.9 mm was performed on DATA. The need of this alignment is also suggested by fig.12. The pulls of the corrected DATA and the Toy MC are compared in fig.26. The good agreement obtained makes the new simulation reliable for checking the effects studied in the following sections.

4.6.1 Radiative emission

The Initial State Radiation lowers, in average, the energy available in the center of mass system, as shown in fig. 27: the production energy of the ϕ meson is not $\sqrt{s}$ but $\sqrt{s'}$. In order to evaluate the effect on the value of the η mass, a MC sample has been produced switching off the ISR simulation and a difference of 104 keV was found on the resulting mass. This imposes to carefully evaluate the systematics due to this effect.
Studied performed for the note [10] have shown that the QED uncertainity in describing the ϕ line shape is negligible. Uncertainity of ϕ line shape in the generator can instead be the source of the main systematic error. In order to evaluate systematics we have simulated 10 points at different $\sqrt{s}$ values and estimated the deviation from the nominal value of the η mass inserted in the generator: $m_\eta = 547.9\ \text{MeV}/c^2$.

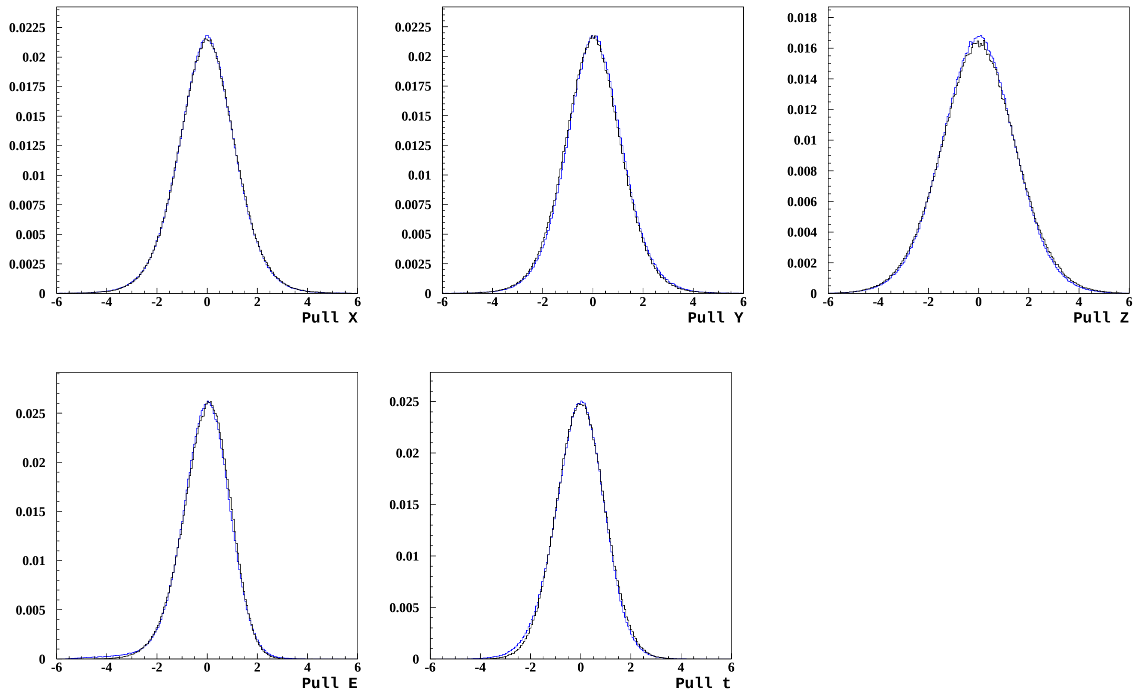

Figure 26: x, y, z, E, t pulls after the correction on DATA and MC.

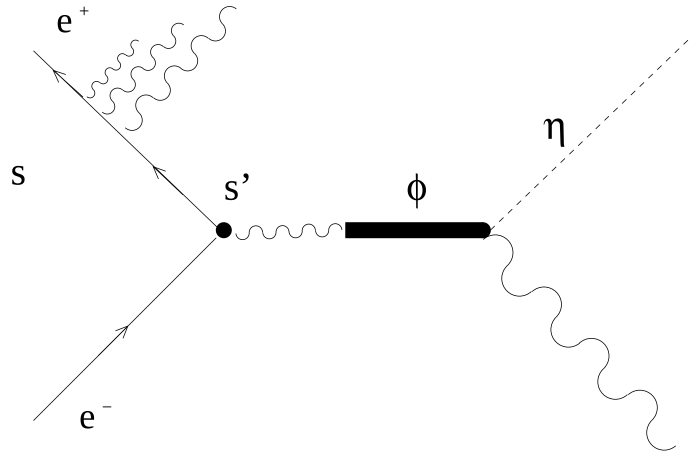

Figure 27: Scheme of radiative emission in the $e^+e^- \to \phi \to \eta\gamma$ process.

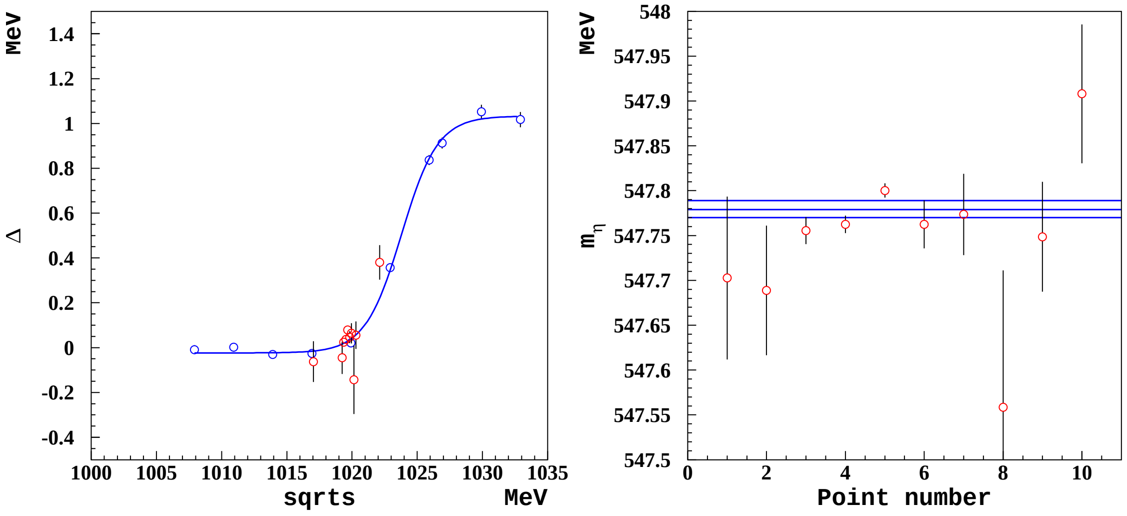

Figure 28: Left: correction to the η mass evaluated by MC as a function of $\sqrt{s}$, blue points MC, blue curve fit, red points DATA; Right: data value after correction. The middle blue line is the mean value while the two line above and below are $+/-$ 1 σ systematic.

In fig. 28 this correction has been shown. The points given by the MC have been fitted with the following function:

$$\Delta_{ISR} : m_{ouput} - m_{input} = \frac{A}{1 + e^{-\frac{(\sqrt{s}-B)}{C}}} + D \qquad (2)$$

the fitted parameters A, B, C, D are shown in table 10. The whole data set has been divided in bins of $\sqrt{s}$. Two off peak points 1017 MeV and 1022 MeV have been used, and the whole on peak data set has been divided in 8 bins of $\sqrt{s}$. The η mass distribution has been fit in each data point and the value has been corrected using the function (2):

$$m_\eta \,\mathrm{corr} = m_{\eta_f it} - \Delta_{ISR}$$

	η		π^0	
Parameter (MeV)	value	error	value	error
A	1.06	0.02	0.85	0.03
B	1023.8	0.04	1028.7	0.2
C	1.40	0.09	2.90	0.16
D	-0.024	0.009	0.081	0.006

Table 10: Fitted paremeters for the correction curve to the η and π^0 mass evaluated on MC .

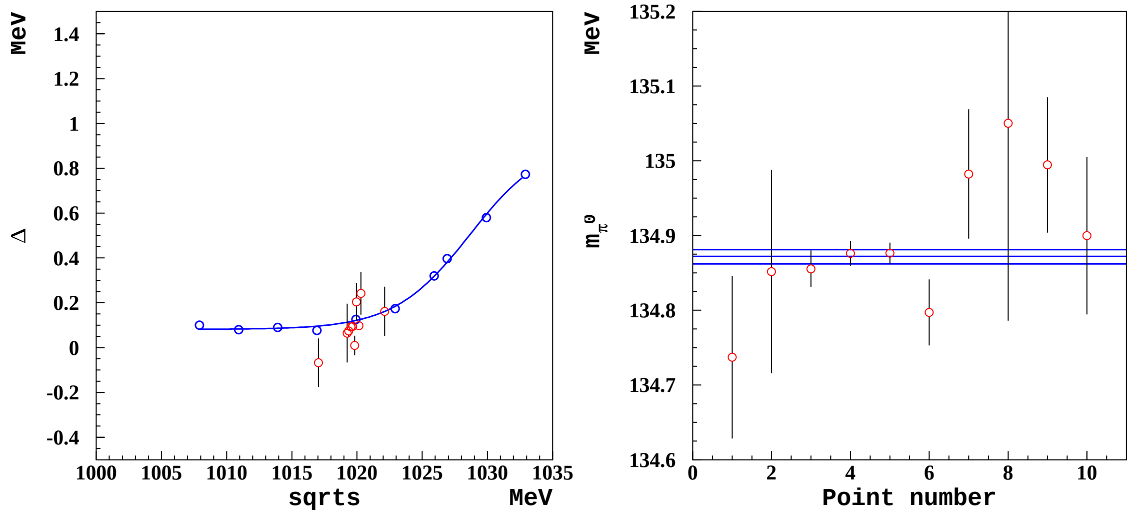

Figure 29: Left: correction to the π^0 mass evaluated by MC as a function of $\sqrt{s}$, blue points MC, blue curve fit, red points DATA; Right: data value after correction. The middle blue line is the mean value while the two line above and below are $+/-$ 1 σ systematic.

The values of $m_{\eta\ corr}$ have been shown in fig.28, right. The mean value has been computed $m_{mean} = 547.779 \pm 0.005$ MeV. The χ^2 obtained from the several measurement is $\chi^2/\text{n.d.f} = 20/9$. The measurements are not statistically compatible and the spread of the measurements is used to evaluate the systematic error due to the ISR simulation in the MC. The spread is evaluated multiplying the error on the mean by a scale factor $s = \sqrt{\chi^2/9}$ obtaining $\sigma_{systISR} = 0.008$ MeV.
The same precedure has been applied for the m_{π^0} measurement. The MC correction curve and the corrected values as a function of $\sqrt{s}$ are shown in fig.29, while the parameters of the fitted curve are shown in table 10. In the π^0 case we obtain $\chi^2/\text{n.d.f} = 9.04/9$ and $\sigma = 0.009$ MeV, so $\sigma_{ISR} = 0.009$ MeV. The ISR systematic error on the ratio of two masses has been computing correcting the π^0 and η mass with the ISR curve and evaluating again the spread of the point as a function of $\sqrt{s}$. The values are shown in fig. 30. We obtain $\chi^2/\text{n.d.f} = 8.5/9$ and $\sigma_{ISR} = 28 \times 10^{-5}$.

4.7 Effect of the beam energy spread

Also the beam energy spread has been considered as a possible source of systemtics. A simulation was performed in which the beam energy was fixed to the measured value but no difference has been seen on the resulting mass value.

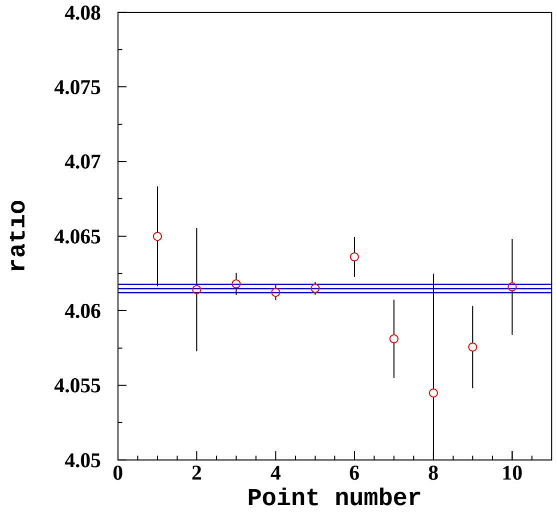

Figure 30: m_η/m_{π^0} as a function of $\sqrt{s}$ after ISR correction. The middle blue line is the mean value while the two line above and below are $+/-$ 1 σ systematic.

5 Systematic effect summary.

The systematic effects studied in this work are summarized in tab. 11. Being the systematic sources independent one from each other we can sum in quadrature all the effects to give the final number in the last row of the table.

6 Global fit to the data.

To check possible variation of the result with the time of the data taking, we have divided the whole data sample in 8 periods. The fit has been performed for the π^0 and the η peak after having corrected each entry in the histogram with the function (2). The χ^2 and the fit probabilities are shown in fig. 31.

The fit probability is reasonable for all periods. So we can fit all the data with a constant value. The results together with the values obtained in the several periods is shown in fig. 32, while the ratio of the two masses is shown in fig. 33.

Very good fit probabilties are obtained, showing the consistence of the result on all of the data periods. The results of these fits are shown in tab. 12. Good fit probability are obtained for all the measurements, this means that the observed fluctuations are just of statistical type and the result is stable against different running condition in 2 years of data taking.

systematic effect	m_η (keV)	m_{π^0} (keV)	$m_\eta/m_{\pi^0} \times 10^{-5}$
Calorimeter energy constants	4	1	5.6
Calorimeter not linearity	4	11	31
Vertex position	4	6	19
Angular uniformity ϕ	15	12	37
Angular uniformity θ	10	44	120
ISR effect	8	9	28
Dalitz plot slope	12	4	15
Dalitz plot cut (constant)	12	1.9	10
χ^2 cut	0.7	4	13
overall	27	49	136

Table 11: Summary of the all evaluated systematic errors.

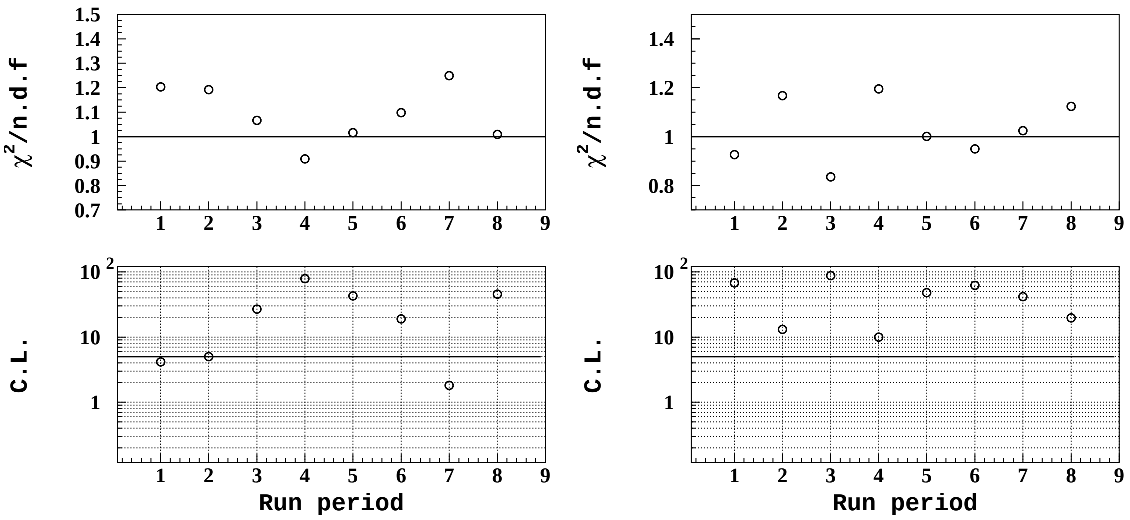

Figure 31: χ^2 (top) and C.L. (bottom) for the η (left) and π^0 (right) mass fit. The data sample has been divided in 8 sub-periods.

Fit results				
	Value	Error	$\chi^2/n.d.f$	C.L
m_η	547791 keV	7 keV	6.9/7	45%
m_{π^0}	134886 keV	12 keV	7.7/7	34%
m_η/m_π	4.0610	0.0004	8.9/7	26%

Table 12: Fit results to the 8 data points.

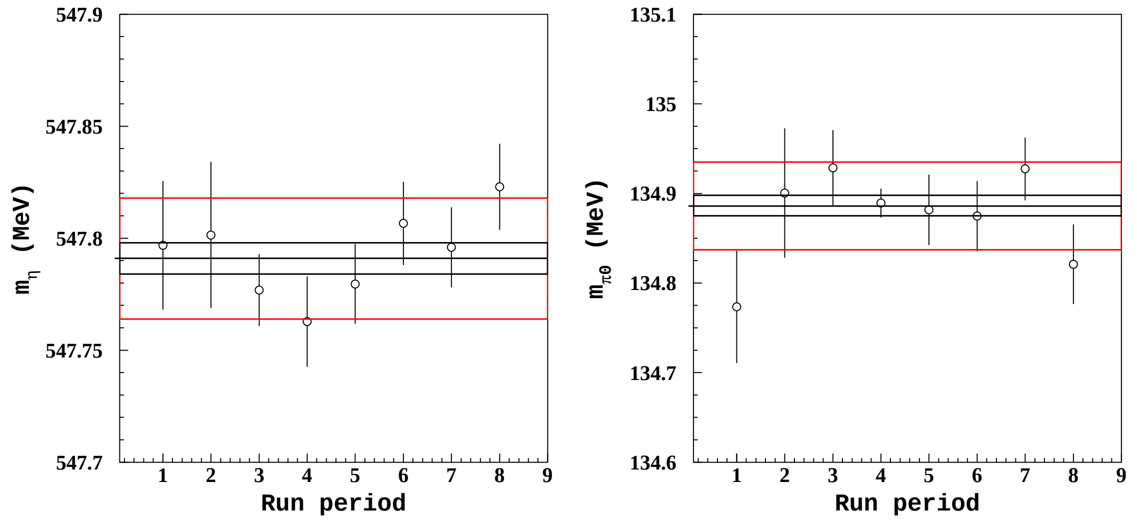

Figure 32: **left** Fit to the η mass, **right** Fit to the π^0 mass. The small rectangle is the fit statistical error while the rectangle is the systematic error.

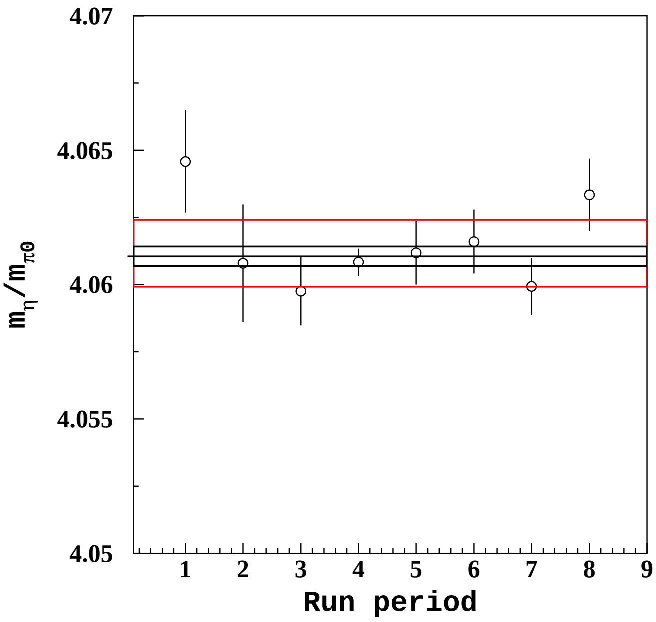

Figure 33: Fit to the mass ratio. The small rectangle is the fit statistical error while the rectangle is the systematic error.

7 Computation of the final result.

We have different ways to extract the value of the η mass.

We can use the ratio of the m_η/m_{π^0},

$$\frac{m_\eta}{m_{\pi^0}} = 4.0610 \pm 0.0004(\text{stat.}) \pm 0.0014(\text{syst.}),$$

from which using the PDG2006[1] value for the π^0 mass ($m_{\pi^0} = 134976.6 \pm 0.6$ keV) we obtain: $m_\eta = 548140 \pm 50(\text{stat.}) \pm 190(\text{syst.})$ keV.

Since the absolute scale is given by the m_ϕ measurement from CMD-2 we can consider our two measurements as follows:

$$\frac{m_\eta}{m_{\phi CMD2}} = 0.537403 \pm 0.000007(\text{stat.}) \pm 0.000026(\text{syst.}) \pm 0.000006(m_\phi \quad \text{stat.})$$

and

$$\frac{m_{\pi^0}}{m_{\phi CMD2}} = 0.132328 \pm 0.000012(\text{stat.}) \pm 0.000048(\text{syst.}) \pm 0.000001(m_\phi \quad \text{stat.})$$

therefore we can extract the π^0 and η mass using the value of CMD-2 $m_\phi = 1019.483 \pm 0.011(\text{stat.}) \pm 0.025(\text{syst.})$.

$$\begin{array}{llll} m_{\pi^0} & = 134906 & \pm 12(\text{stat.}) & \pm 48(\text{syst.}) & \pm 1(m_\phi \quad \text{stat.}) + \\ & & \pm 1.4(\text{CMD2stat.}) & \pm 3(\text{CMD2syst.}) & \text{keV} \\ \\ m_\eta & = 547874 & \pm 7(\text{stat.}) & \pm 26(\text{syst.}) & \pm 6(m_\phi \quad \text{stat.}) + \\ & & \pm 6(\text{CMD2stat.}) & \pm 14(\text{CMD2syst.}) & \text{keV} \end{array}$$

Summing in quadrature independently statistical and systematic error we obtain:

$$m_{\pi_0} = 134.906 \pm 0.012(\text{stat.}) \pm 0.048(\text{syst.}) \quad \text{MeV}$$

$$m_\eta = 547.873 \pm 0.007(\text{stat.}) \pm 0.031(\text{syst.}) \quad \text{MeV}$$

We can compare the π^0 mass to the PDG06 value obtaining an agreement at 1.4 σ level. This agreement can be considered a good check of the whole procedure. The measured η mass is compared with previous measurements in fig. 34. This result confirms the measured value of the NA48 at 0.6σ with an error reduced by a factor 2 and is 11σ away from the GEM result, it is also compatible, at 1.4σ level, with the less accurate and recently published CLEO result [12]. Here we stress that this is today the most accurate determination of the η mass and that together with results from CLEO and NA48 definitively clarify the experimental situation. On the other sides, we note that the average of all old measurents except GEM (RL 74, SATURNE 92, MAMI 95D) is $M_\eta = 547.30 \pm 0.12$, that is 4.8 σ away from the KLOE result. The two sets of measurement, higher versus lower, were done with different technique. In particular, in NA48, GEM and CLEO the η is produced in vacuum while in the other case the η is produced in nuclear matter. Morever, in the lower measurements involving missing mass techniques or cross section threshold determinattion, the η mass was measured at production time in nuclear matter. This discrepancy could be explained either by an underestimate of the experimental systematic error or, and this would be more attractive, by some still unknown physical process in the η production mechanism.

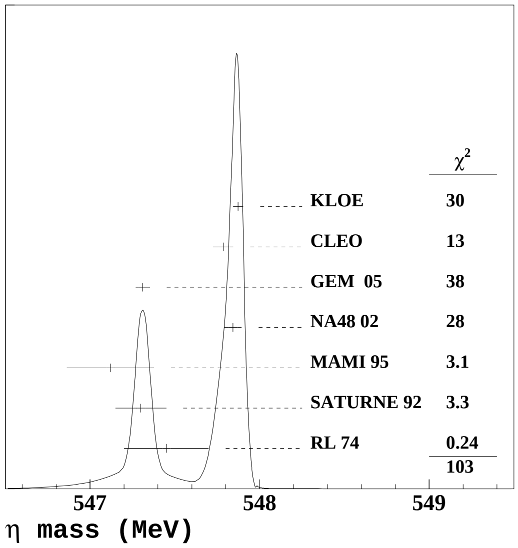

Figure 34: η mass measurements, see text for the references. The continuous line has been computed using the PDG procedure [1], pag. 14.

References

[1] W.-M. Yao et al., J. Phys. G33, 1 (2006)

[2] A. Duane *et al.*, Phys. Rev. Lett. 32, 425 (1974)

[3] F. Plouin *et al.*, Phys. Lett. B 276, 526 (1992)

[4] B. Krusche *et al.*, Z. Phys. A 351, 237b

[5] A. Lai *et al.*, Phys. Lett. B 533, 196 (2002)

[6] M. Abdel-Bary *et al.*, Phys. Lett. B 619, 281 (2005)

[7] B. Di Micco, Phd. Thesis "Measurement of the Branching Ratio $\eta \to \pi^0\gamma\gamma$ and upper limit on the decay $\eta \to \gamma\gamma\gamma$ with the KLOE experiment", Università degli Studi di Roma Tre, Roma, (2005)

[8] S. Dell'Agnello, M. Primavera, KLOE memo n. 202, (2000)

[9] M. Adinolfi *et al*, Nucl. Instrum. Meth. A 482, 364 (2002)

[10] M. Antonelli, M. Dreucci, KLOE note n. 181 (2002)

[11] R.R. Akhmetshin *et al.*, Phys. Lett. B578, 285 (2004)

[12] D.H. Miller *et al.*, arXiv:0707.1810v1

[13] V.L. Eletsky and B.L. Ioffe, Phys. Rev. Lett. 78, 1010 (1997)